Phase Transformations in Pulsed Laser Deposited Nanocrystalline Tin Oxide Thin Films

Haiyan Fan and Scott A. Reid*

Department of Chemistry, Marquette University, Milwaukee, Wisconsin 53201-1881

Received August 20, 2002. Revised Manuscript Received November 11, 2002

Thin SnO_x films have been synthesized with the method of pulsed laser deposition and their microstructure examined using X-ray diffraction (XRD). The films were amorphous as grown and subjected to postdeposition annealing in air to various temperatures. The litharge phase of SnO (α-SnO) was found only in films grown at laser fluences greater than ∼1.9 × 10^8 W cm^{-2} and was stable in the temperature range of ∼300−500 °C. Formation of the orthorhombic SnO_2 phase (*o*-SnO_2) was correlated with film thickness, being found in thicker films (basically, >500 nm) at ∼500 °C, and was stable up to ∼900 °C. These observations are examined in light of results from time-of-flight mass spectrometric analysis of the ablated plume. The average grain size of these films, as determined from the XRD peak widths, was found to increase with increasing laser fluence and film thickness.

Introduction

SnO_2 is a prototypical optically transparent n-type semiconductor that is widely used as a base material for the sensing of reducing gases,[1−3] and thin films have been synthesized by various means including evaporation,[4] sputtering,[5] chemical vapor deposition,[6] sol−gel processes,[7] and pulsed laser deposition (PLD).[8−19] Generally, solid SnO_2 is found in a tetragonal (rutile) structure (cassiterite, *r*-SnO_2). A metastable orthorhombic phase (*o*-SnO_2) was observed initially after quenching from a high pressure (15.8 GPa)[20] and subsequently in various thin film and powder experiments[17,21−23] under conditions that were not always associated with high pressure. Kaplan et al. found this phase in films grown by deposition of ionized tin atoms in the presence of oxygen at substrate temperatures of 350−500 °C and when amorphous films were subjected to rapid thermal annealing.[21] They attributed its formation in the first case to the energetic nature of ion deposition, and in the second case to the relatively high density of the amorphous phase. In another study, Shek et al. observed *o*-SnO_2 when tin particles with an average size of 6 nm were oxidized[22] and suggested that *o*-SnO_2 formation was favored in the annealing of disordered (amorphous or nanoparticle) tin oxide under oxygen-deficient conditions.

In our previous research,[17] thin films were deposited on Si(001) substrates using 532-nm PLD from a compressed SnO_2 target. It was found by XRD that the films were initially amorphous and crystallized in a series of steps upon subsequent postdeposition annealing. For one set of films, crystallization into the litharge phase of SnO (α-SnO) occurred at 300 °C, followed by transformation to the orthorhombic and cassiterite phases of SnO_2. The fraction of *o*-SnO_2 reached ∼50% at 700 °C, with complete conversion to *r*-SnO_2 at ∼1150 °C. A second set of films subjected to the same heat treatment did not show the litharge and orthorhombic phases and were oxidized directly to *r*-SnO_2 at 1150 °C. The films exhibiting the litharge and orthorhombic phases were ∼3 times thicker, being grown at a higher laser fluence. Our motivation for this work was to clarify

* To whom correspondence should be addressed. E-mail: Scott.Reid@mu.edu.

(1) Madou, M. J.; Morrison, S. R. *Chemical Sensing with Solid State Devices*; Academic: Boston, 1989.
(2) Iida, H.; Shiba, N.; Mishuku, T.; Karasawa, H.; Ito, A.; Yamanaka, M.; Haiyashi, Y. *IEEE Electron Device Lett.* **1983**, *EDL-4*, 157.
(3) Takahata, K. In *Chemical Sensor Technology*; Seiyama, T., Ed.; Elsevier: Amsterdam, 1988; p 39.
(4) D'Almeida, K.; Bernede, J. C.; Marsillac, S.; Godoy, A.; Diaz, F. R. *Synth. Met.* **2001**, *122*, 127.
(5) Chen, J. S.; Li, H. L.; Huang, J. L. *Appl. Surf. Sci.* **2002**, *187*, 305.
(6) Rajaram, P.; Goswami, Y. C.; Rajagopalan, S.; Gupta, V. K. *Mater. Lett.* **2002**, *54*, 158.
(7) Shoyama, M.; Hashimoto, N. *Chem. Sens.* **2001**, *17*, 10.
(8) Shatokhin, A. N.; Putilin, F. N.; Safonova, O. V.; Rumyantseva, M. N.; Gas'kov, A. M. *Inorg. Mater.* **2002**, *38*, 374.
(9) Dominguez, J. E.; Pan, X. Q.; Fu, L.; Van Rompay, P. A.; Zhang, Z.; Nees, J. A.; Pronko, P. P. *J. Appl. Phys.* **2002**, *91*, 1060.
(10) Hu, W. S.; Lui, Z. G.; Wu, Z. C.; Feng, D. *Mater. Lett.* **1996**, *28*, 369.
(11) Vispute, R. D.; Godbole, V. P.; Chaudhari, S. M.; Kanetkar, S. M.; Ogale, S. B. *J. Mater. Res.* **1988**, *3*, 1180.
(12) Godbole, V. P.; Vispute, R. D.; Chaudhari, S. M.; Kanetkar, S. M.; Ogale, S. B. *J. Mater. Res.* **1990**, *5*, 372.
(13) Lal, R.; Grover, R.; Vispute, R. D.; Viswanathan, R.; Godbole, V. P.; Ogale, S. B. *Thin Solid Films* **1991**, *206*, 88.
(14) Dai, C. M.; Su, C. S.; Chuu, D. S. *Appl. Phys. Lett.* **1990**, *57*, 1879.
(15) Morosova, N. V.; Gas'kov, A. M.; Kuznetsova, T. A.; Putilin, F. N.; Rumyantseva, M. N.; Shatnov, V. I. *Inorg. Mater.* **1996**, *32*, 292.
(16) Hu, W. S.; Liu, Z. G.; Zheng, J. G.; Hu, X. B.; Guo, X. L.; Gopel, W. *J. Mater. Sci.: Mater. Electron.* **1997**, *8*, 155.
(17) Lamelas, F. J.; Reid, S. A. *Phys. Rev. B: Condens. Matter Mater. Phys.* **1999**, *60*, 9347.
(18) Dominguez, J. E.; Fu, L.; Pan, X. Q. *Appl. Phys. Lett.* **2001**, *79*, 614.
(19) Pan, X. Q.; Fu, L.; Dominguez, J. E. *J. Appl. Phys.* **2001**, *89*, 6056.
(20) Haines, J.; Léger, J. M. *Phys. Rev. B: Condens. Matter Mater. Phys.* **1997**, *55*, 11114.
(21) Kaplan, L.; Ben-Shalom, A.; Boxman, R. L.; Goldsmith, S.; Rosenberg, U.; Nathan, M. *Thin Solid Films* **1994**, *253*, 1.
(22) Shek, C. H.; Lai, J. K. L.; Lin, G. M.; Zheng, Y. F.; Liu, W. H. *J. Phys. Chem. Solids* **1997**, *58*, 13.
(23) Lu, B.; Wang, C.; Zhang, Y. *Appl. Phys. Lett.* **1997**, *70*, 717.

10.1021/cm0208509 CCC: $25.00
Published on Web 00/00/0000

Table 1. Phase Transformations Observed in the Postdeposition Annealing of SnO_x Films Grown at Different Laser Fluences and with Different Thicknesses

laser fluence (10^7 W cm^{-2})	average film thickness (nm)	phases observed
8	520	*r*-SnO_2
	1020	*o*-SnO_2, *r*-SnO_2
15	490	*o*-SnO_2, *r*-SnO_2
	560	*o*-SnO_2, *r*-SnO_2
26	310	α-SnO, *r*-SnO_2
	530	α-SnO, *o*-SnO_2, *r*-SnO_2
36	270	α-SnO, *r*-SnO_2
	710	α-SnO, *o*-SnO_2, *r*-SnO_2

the relationship between the phase transformations observed in postdeposition annealing and the fabrication conditions.

Experimental Section

SnO_2 films were deposited on unheated Si(001) substrates by 532-nm PLD from a SnO_2 target. A detailed description of the deposition system was given in ref 17. The laser beam struck the target along the surface normal with a circular spot of 1-mm diameter. The target was prepared by pressing 10 g of SnO_2 powder (>99.99%) into a pellet 1 in. in length and 0.5 in. in diameter, under a typical pressure of 6000 psi. The pellet was sintered in a furnace (Thermolyne 1300) at 1150 °C for 72 h and mounted on a motor-controlled linear-rotary motion feedthrough that rotated and translated the target simultaneously. The pressure in the growth chamber was typically $\sim 3 \times 10^{-7}$ Torr.

Postdeposition annealing was carried out in the furnace described above. All samples were placed in an open crucible and heated at a temperature interval of 50 °C. The soak time was typically 2−3 h. No obvious change in the appearance of the films was observed during heat treatment. X-ray diffraction (XRD) measurements were performed with a powder diffractometer in parafocusing Bragg-Bretano geometry and a Cu tube source operated at 1 kW. The counting time was 45 s per point, and the typical scan range was 20−60° in 2θ with a step size of 0.05°. The longitudinal resolution of the diffractometer at $q = 2.0$ Å^{-1} was approximately 0.012 Å^{-1}. The diffraction peaks were fit to a Lorentzian line shape function using nonlinear least squares (PSIplot) and calibrated against a Si powder standard. The accuracy of the determined crystal constant (d) was estimated to be ~0.1%.[17]

The films fabricated by PLD are optically transparent and have very little absorption above 400 nm. To determine film thickness, spectral reflectance measurements were conducted using a home-built reflectance spectrometer consisting of a 100 W QTH (quartz−tungsten−halogen) lamp (Oriel) and fiber optic coupled CCD spectrometer (Control Development). We obtained reflectance spectra at two angles of incidence, and the film thickness and wavelength dependent index of refraction were obtained from the reflectance maxima/minima following a method recently described.[24,25] For comparison, the film thickness was also measured with a profilometer (Alpha-steep100, Tencor), and a comparison of results from the two methods leads to an estimated error in film thickness of ±20 nm.

Results and Discussion

In our previous report,[17] one set of films grown at a fluence of $\sim 2.5 \times 10^8$ W cm^{-2} exhibited the α-SnO phase after postdeposition annealing at 300 °C, while a second set grown at a fluence of $\sim 1.3 \times 10^8$ W cm^{-2} did not show any trace of this phase. To verify this result and understand its origins, we grew a set of films over a range of fluences, and the results are summarized in Table 1. It is apparent that α-SnO only appears in films grown at laser fluences above $\sim 2 \times 10^8$ W cm^{-2}, irrespective of film thickness. Examples are shown in Figures 1 and 2, which display the XRD patterns at different stages of annealing for films grown at 7.7×10^7 W cm^{-2} (Figure 1) and 3.6×10^8 W cm^{-2} (Figure 2). From the XRD patterns, the film grown at 7.7×10^7 W cm^{-2} exhibits only the cassiterite phase, which appears at ~500 °C. For the film grown at 3.6×10^8 W cm^{-2}, crystallization into α-SnO is observed at ~300 °C, followed by the orthorhombic phase of SnO_2 at ~700 °C. At ~1100 °C, the film was completely transformed into *r*-SnO_2.

These data confirm the results of our initial report[17] and demonstrate that formation of α-SnO is dependent

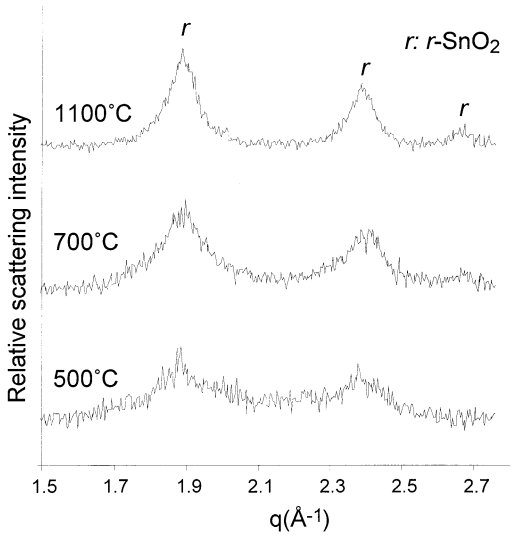

Figure 1. XRD patterns at three different annealing stages for a SnO_x thin film grown on Si(001) by the ablation of an SnO_2 target at 532 nm. The laser fluence was 8×10^7 W cm^{-2}, and the average film thickness is 520 nm.

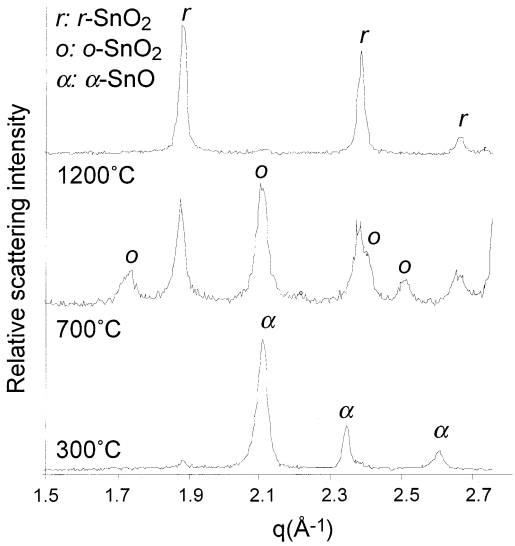

Figure 2. XRD patterns at three different annealing stages for a SnO_x thin film grown on Si(001) by the ablation of an SnO_2 target at 532 nm. The laser fluence was 3.6×10^8 W cm^{-2}, and the average film thickness is 710 nm.

(24) Manifacier, J. C.; Gasiot, J.; Fillard, J. P. *J. Phys. E* **1976**, *9*, 1002.
(25) Ohlidal, I.; Franta, D.; Ohlidal, M.; Navratil, K. *Appl. Opt.* **2001**, *40*, 5711.

on fluence rather than film thickness. Our TOFMS studies[26,27] shed light on the origin of this dependence. A detailed description of the fluence dependence of the relative neutral yields and neutral energetics will be presented elsewhere,[27] and here we briefly summarize the key results. Previously, we found that SnO and Sn_2O_2 were the primary neutral gas-phase species produced from SnO_2 ablation at 532 nm.[26] The relative yield of neutral Sn-containing species was found to increase exponentially for pulse energies below $\sim 1.9 \times 10^8$ W cm^{-2} and saturate at higher fluences.[26] Subsequent studies have shown that the yield of larger clusters such as Sn_2O_2 and Sn_4O_4 increases in the saturated region, while the yield of unoxidized species such as Sn and Sn_2 decreases. In other words, the Sn:O stoichiometry of neutral species in the plume increases at higher laser fluences. In contrast, the peak kinetic energy of the primary neutral ablated species is insensitive to laser fluence in this range. These results indicate that the initial Sn:O stoichiometry of the amorphous film may play a significant role. Support for this hypothesis is provided in the work of Muranaka and co-workers,[28] who observed the formation of α-SnO from initially amorphous SnO_x ($x = 1.3-1.5$) films annealed in a nitrogen atmosphere. However, when the films were annealed in air, complete oxidation occurred prior to crystallization, and only *r*-SnO_2 was observed.

As noted in our initial report,[17] the formation of *o*-SnO_2 in a thin film is unusual. To identify the conditions necessary for its formation, we refer again to Table 1, which shows that *o*-SnO_2 is observed only for the thicker films grown at each fluence and is not correlated with the formation of α-SnO. We considered several factors that might be responsible for the formation of this phase and its correlation with film thickness. These are summarized below.

1. Intrinsic or Annealing Induced Macroscopic Strain. In the work of Proden et al.,[29] epitaxial strain at the film−substrate interface was invoked as a possible route to formation of *o*-SnO_2. Epitaxial strains should be less important in our randomly oriented polycrystalline films, but as a test of the importance of film−interface stress, we grew sets of films of similar thickness under the same deposition conditions on three different single-crystal substrates: silicon (linear coefficient of thermal expansion [CTE] $= 2.6 \times 10^{-6}$ K^{-1}),[30] quartz (CTE(||) $= 8.0 \times 10^{-6}$ K^{-1}, CTE(⊥) $= 13.4 \times 10^{-6}$ K^{-1}),[31] and sapphire (CTE(||) $= 5.6 \times 10^{-6}$ K^{-1}, CTE(⊥) $= 5.0 \times 10^{-6}$ K^{-1}).[32] After postdeposition annealing, the *o*-SnO_2 phase was found in all three films. We also looked for shifts in peak positions in XRD spectra taken at different stages of annealing. Table 2 provides a summary of the measured *d* spacings, and their deviation from the literature values, for the *r*-SnO_2 (110) and (101) reflections of a film at three different annealing stages. Consistent with our previous results,[17] the deviations are within the precision of our measurements, and no obvious trend is observed. As a test for inherent strain in films that exhibited the orthorhombic phase, we determined the peak positions of the *r*-SnO_2 (110) and (101) reflections at the end of the annealing cycle in two films of different thickness grown at the same fluence, one exhibiting the orthorhombic phase and the other not. The fit parameters are compared in Table 3 with the literature values for unstrained samples.[20] Again, no obvious deviation or dependence on film thickness is observed.

Table 2. Comparison of Measured (d_m) and Literature (d_l) *d* Spacings Determined from the XRD Peak Positions of *r*-SnO_2 Reflections for a Film Grown at a Fluence of 8 × 10^7 W cm^{-2}

annealing temperature	*r*-SnO_2 reflection	d_m	$(d_m - d_l)/d_l$ (%)
500 °C	110	3.358	0.2
	101	2.654	0.4
700 °C	110	3.351	0.0
	101	2.640	0.0
1100 °C	110	3.356	0.2
	101	2.647	0.2

Table 3. XRD Peak Positions of *r*-SnO_2 Phase Reflections for Two Films of Different Thicknesses Grown at a Fluence of 8 × 10^7 W cm^{-2} [a]

film thickness	*r*-SnO_2 reflection	q_l (Å^{-1})	q_m (Å^{-1})	d_m (Å)	$(d_m - d_l)/d_l$ (%)	phase(s) observed
520	110	1.875	1.875	3.349	0.0	*r*-SnO_2
	101	2.377	2.378	2.641	0.0	
1020	110	1.875	1.873	3.353	0.1	*o*-SnO_2,
	101	2.377	2.375	2.644	0.1	*r*-SnO_2

[a] Key: q_m are the measured peak positions obtained as described in the text, q_l are the peak positions from the literature for unstrained samples, and d_m and d_l are the measured and literature *d* spacings.

2. Microscopic Strain. Microscopic strains can be evidenced by the inhomogeneous broadening of peak profiles in XRD. As the XRD peak profiles of all our films were well fit by a Lorentzian line shape function (Figure 3), we found no obvious evidence for microscopic strains in our films.

3. Oxidation Conditions. The orthorhombic phase was previously observed as an intermediate in the oxidation of tin particles under oxygen-deficient conditions and was drastically suppressed in an oxygen-enriched environment.[22] Thus, *o*-SnO_2 may be favored in annealing under oxygen-deficient conditions. Geurts et al.[33] showed that oxidation of SnO_x films proceeds initially through internal oxygen redistribution, and at higher temperatures by diffusion of external oxygen, a conclusion supported by recent experiments.[19] (Note that *o*-SnO_2 was not observed in these studies, as the film thickness was in each case well below the threshold value we observe.) Given that the extent of oxygen diffusion into the film interior at a given temperature will depend on film thickness, the observed dependence indicates that *o*-SnO_2 may be formed preferentially in the interior of the thicker films. Our XRD annealing studies[17] show similar appearance temperatures for *o*-SnO_2 and *r*-SnO_2, and a similar rate of increase in intensity with temperature up to ~650 °C, consistent with simultaneous growth of these phases.

(26) Reid, S. A.; Ho, W.; Lamelas, F. J. *J. Phys. Chem. B* **2000**, *104*, 5324.
(27) Fan, H.; Ho. W.; Reid, S. A., unpublished results.
(28) Muranaka, S.; Yoshichika, B.; Takada, T. *Nippon Kagaku Kaishi* **1987**, *11*, 1886.
(29) Prodan, A.; Vene, V.; Sevsek, F.; Hudomalj, M. *Thin Solid Films* **1987**, *147*, 313.
(30) Okaji, M. *Int. J. Thermophys.* **1988**, *9*, 1101.
(31) Amatuni, A. N.; Shevchenko, E. B. *Izmer. Tekh.* **1966**, *10*, 17.
(32) Yim. W. M.; Paff, R. J. *J. Appl. Phys.* **1974**, *45*, 1456.
(33) Geurts, J.; Rau, S.; Richter, W.; Schmitte, F. J. *Thin Solid Films* **1984**, *121*, 217.

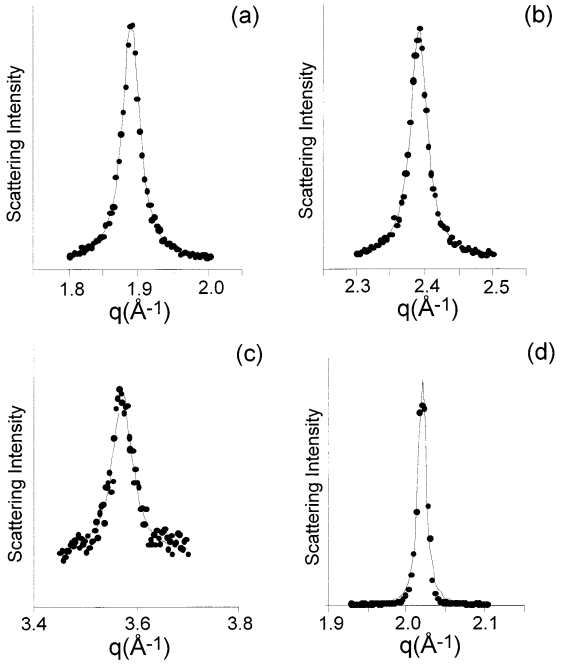

Figure 3. Measured intensity (dots) and Lorentzian fits (curves) for the peaks of the *r*-SnO_2 phase [(a)−(c)] for a SnO_x thin film grown by the ablation of the SnO_2 target at 532 nm. The laser fluence was 3.6×10^8 W cm^{-2}, and the average film thickness is 270 nm. Key: (a) 110 reflection; (b) 101 reflection; (c) 211 reflection; (d) Si(111).

In summary, we have not identified any intrinsic or annealing-induced strain that might be responsible for the formation of the high-pressure *o*-SnO_2 phase in our films. However, our results are not inconsistent with the hypothesis that *o*-SnO_2 is favored in the annealing of disordered tin oxide films under oxygen-deficient conditions. This hypothesis could be further tested by micro-Raman imaging of our films,[34] and we are presently seeking to acquire Raman spectra of the orthorhombic phase.

Finally, we noticed an obvious dependence of the XRD peak widths on laser fluence and film thickness that is readily seen by comparing Figures 1 and 2. Figure 3 displays expanded views of the *r*-SnO_2 (110), (101), and (211) together with the 111 reflection of a Si powder standard. In each case, the fit to a Lorentzian function is shown as a solid line. Following our previous work,[17] the peak width was calculated from the equation $\Delta q_m^2 = \Delta q_{int}^2 + \Delta q_{ins}^2$, where Δq_m is the measured fwhm and Δq_{ins} is the instrumental width determined from the Si standard ($\Delta q_{in} = 0.012$ Å^{-1} when fitting with Lorentzian function). This intrinsic resolution was assumed for all peaks in the range of $q = 1.6-2.8$. The average grain size was then calculated as $2\pi/\Delta q_{in}$,[35] and the values are listed in Table 4. With the caveat that this method gives only a crude measure of the average grain size,[35] we notice that the average grain size increases with increasing laser fluence for films of similar thickness

Table 4. Dependence of the Average Grain Size as Determined from the XRD Peak Widths on Laser Fluence and Film Thickness; Stated Uncertainty Represents One Standard Error

laser fluence (10^7 W cm^{-2})	film thickness (nm)	average grain size (Å)
8	520	70 ± 3
	1020	234 ± 2
15	590	247 ± 3
26	530	360 ± 5
36	270	201 ± 5
	710	358 ± 6

(520, 590, and 530 nm), which may result from changes in the energy content of the ablated material. Song reported a slight increase in grain size with increasing oxygen ion energy for SnO_x films grown by reactive-ion-assisted deposition.[36] As shown in Table 4, the average grain size as determined from the XRD peak widths is also found to depend on film thickness. With increasing thickness, the coherent growth of new grains in the film is less probable than aggregation to the existing grains, which leads to a larger grain size.[37] It is highly desirable in future work to probe these films with transmission electron microscopy (TEM) or atomic force microscopy (AFM) to confirm these observations and better quantify the dependence of film microstructure on process variables.

Conclusions

For SnO_x films grown via PLD at 532 nm, we have demonstrated the conditions necessary to observe α-SnO and *o*-SnO_2 as intermediate phases. The litharge phase of SnO occurs only in films grown at laser fluences greater than $\sim 1.9 \times 10^8$ W cm^{-2} and is stable in the temperature range of ∼300−500 °C. We suggest on the basis of TOFMS analysis of the ablated plume that formation of α-SnO is dependent on the stoichiometry of the as-deposited film. Thinner films (thickness less than ∼500 nm) can be directly oxidized to *r*-SnO_2, while thicker films exhibit both *o*-SnO_2 and *r*-SnO_2, with complete conversion to *r*-SnO_2 at temperatures above ∼900 °C. We have not identified any intrinsic or annealing-induced strains in our films and suggest following the work of Shek et al.[22] that formation of *o*-SnO_2 may occur in annealing under oxygen-deficient conditions.

Acknowledgment. The authors acknowledge the donors of the Petroleum Research Fund, administered by the American Chemistry Society, for support of this work, and thank Frank Lamelas and Jeanne Hossenlopp for useful discussions. The assistance of Lizhong Jiang in conducting profilometry measurements, Yu Wang in the generation of code to analyze the reflectance spectra, and Joe Collins in obtaining the XRD measurements is gratefully acknowledged.

CM0208509

(34) Sangaletti, L.; Depero, L.; Allieri, B.; Pioselli, F.; Comini, E.; Sberveglieri, G.; Zocchi, M. *J. Mater. Res.* **1998**, *13*, 2457.

(35) Gullity, B. D. *Elements of X-ray diffraction*, 2nd ed.; Addison-Wesley: Torrance, 1978.

(36) Song, S.-K. *Phys. Rev. B: Condens. Matter Mater. Phys.* **1999**, *60*, 11137.

(37) Bender, M.; Katsarakis, N.; Gagaoudakis, E.; Hourdakis, E.; Douloufakis, E.; Cimalla, V.; Kiriakidis, G. *J. Appl. Phys.* **2001**, *90*, 5382.